Am J Cancer Res 2026;16(3):1215-1230
www.ajcr.us /ISSN:2156-6976/ajcr0171726

Original Article

THAP7-AS1 orchestrates IGF2BP3-m^{6}A-dependent CCN2 mRNA stabilization to promote lymphatic metastasis in bladder cancer

Qiuyan Li[1,2*], Junjie Bai[1,2*], Shiwen Zheng[3*], Jiaxuan Liao[1,2], Zesong Yang[1,2], Wanghai Cai[1,2], Jiexiang Lin[1,2], Liefu Ye[1,2]

[1]Shengli Clinical College of Fujian Medical University, Fuzhou 350001, Fujian, P. R. China; [2]Department of Urology, Fuzhou University Affiliated Provincial Hospital, Fuzhou 350001, Fujian, P. R. China; [3]Department of Laboratory Medicine, West China Xiamen Hospital, Sichuan University, Xiamen 361022, Fujian, P. R. China. [*]Equal contributors and co-first authors.

Received January 28, 2026; Accepted March 25, 2026; Epub March 25, 2026; Published March 30, 2026

Abstract: Lymphatic dissemination is a major cause of treatment failure in muscle-invasive bladder cancer (MIBC), yet the RNA circuits linking post-transcriptional regulation to lymphatic metastasis remain incompletely defined. Here, we identify THAP7-AS1 as a predominantly cytoplasmic long noncoding RNA that is markedly upregulated in lymph node (LN) metastatic bladder cancer (BCa) and is associated with poor clinical outcome. Functionally, THAP7-AS1 promotes invasion and transendothelial migration in vitro and enhances LN metastasis in vivo. Mechanistically, THAP7-AS1 interacts with the m^{6}A reader IGF2BP3 and facilitates IGF2BP3 association with CCN2 mRNA, thereby promoting m^{6}A-dependent stabilization of CCN2 transcripts and increasing CCN2 protein abundance. Genetic depletion of IGF2BP3 or CCN2 abrogates THAP7-AS1-driven invasive and metastatic phenotypes, whereas CCN2 re-expression partially rescues the effects of THAP7-AS1 silencing. Collectively, these findings define a THAP7-AS1-IGF2BP3-m^{6}A-CCN2 axis that couples post-transcriptional mRNA stabilization to lymphatic metastasis and nominate THAP7-AS1 as a potential biomarker and therapeutic target in BCa.

Keywords: Lymphatic metastasis, THAP7-AS1, N6-methyladenosine (m^{6}A), IGF2BP3, CCN2

Introduction

Lymphatic dissemination is a major determinant of treatment failure and mortality in muscle-invasive bladder cancer (MIBC) [1-3]. Despite advances in surgical techniques and perioperative therapy, patients with lymph node (LN)-positive disease continue to experience early recurrence and poor survival, underscoring the need to define the molecular circuits that license tumor cells to invade, traverse lymphatic endothelium, and establish nodal metastases [1-3]. Current clinicopathological risk stratification primarily relies on stage and grade, which imperfectly capture the biological heterogeneity of BCa and provide limited insight into the RNA-based programs that couple tumor cell-intrinsic reprogramming to lymphatic spread3. A more refined understanding of these post-transcriptional networks is essential for identifying biomarkers that predict LN involvement and for unveiling druggable nodes that constrain lymphatic metastasis.

Long noncoding RNAs (lncRNAs) have emerged as key regulators of cancer progression by acting as molecular scaffolds, decoys, and guides within ribonucleoprotein complexes [4, 5]. Beyond their nuclear roles in chromatin and transcriptional regulation, cytoplasmic lncRNAs are increasingly recognized as critical modulators of mRNA stability and translation, often by engaging RNA-binding proteins and the epitranscriptomic machinery [4, 6]. N6-methyladenosine (m^{6}A) is the most abundant internal modification on eukaryotic mRNA and shapes RNA fate by recruiting dedicated reader proteins [7-9]. Among these, IGF2BP family members, IGF2BP3 in particular, stabilize a subset of m^{6}A-modified transcripts encoding oncogenic drivers and pro-metastatic factors [9, 10]. IGF2BP3 is frequently overexpressed in solid

https://doi.org/10.62347/WGQA3188

tumors, including BCa, and correlates with aggressive clinicopathological features [11, 12]. Yet how specific lncRNA-IGF2BP3-mRNA axes are wired to support invasion and lymphatic metastasis in BCa remains poorly defined.

CCN2 is a secreted matricellular protein implicated in extracellular matrix remodeling, angiogenesis and tumor invasion, and has been linked to metastatic progression in multiple malignancies [13-15]. However, the post-transcriptional mechanisms governing CCN2 expression in BCa, and whether CCN2 serves as an effector of lncRNA-driven epitranscriptomic regulation, remain unclear. THAP7-AS1 is a long noncoding RNA with emerging roles in tumor biology, but its expression pattern, function and mechanistic partners in BCa have not been systematically characterized. In particular, it is unclear whether THAP7-AS1 participates in organizing m^{6}A reader complexes on specific effector transcripts to drive lymphatic dissemination [16-18].

Mechanistically, THAP7-AS1 binds the m^{6}A reader IGF2BP3 and CCN2 mRNA, assembling a ternary ribonucleoprotein complex in the cytoplasm. This THAP7-AS1-IGF2BP3-m^{6}A axis selectively stabilizes CCN2 transcripts by facilitating IGF2BP3 engagement with m^{6}A-modified sites within the CCN2 3'UTR, thereby augmenting CCN2 expression. Genetic disruption of IGF2BP3 or CCN2 abrogates THAP7-AS1-driven invasive and lymphatic metastatic phenotypes. Collectively, our findings define a THAP7-AS1-centered post-transcriptional module that couples m^{6}A-dependent mRNA stabilization to lymphatic metastasis and nominate the THAP7-AS1-IGF2BP3-CCN2 axis as a potential biomarker and therapeutic vulnerability in BCa.

Materials and methods

Clinical samples and ethics statement

A total of 200 pairs of BCa tissues and noncancerous adjacent tissues (NAT). These specimens were collected after written informed consent and with approval from the Ethics Committee of Fuzhou University Affiliated Provincial Hospital. The histological type and pathological stage of each clinical sample were independently assessed by three experienced pathologists. Inclusion criteria for enrolled patients: (1) Patients who underwent radical cystectomy or transurethral resection of bladder tumor (TURBT) at Fuzhou University Affiliated Provincial Hospital between January 2016 and December 2020; (2) Histopathologically confirmed primary urothelial carcinoma of the bladder by three independent senior pathologists; (3) Complete clinicopathological and follow-up data available; (4) No preoperative radiotherapy, chemotherapy, immunotherapy, or other anti-tumor treatments received before surgery. Exclusion criteria: (1) Patients with non-urothelial bladder cancer (e.g., squamous cell carcinoma, adenocarcinoma); (2) Patients with a history of other malignant tumors; (3) Patients with severe systemic diseases or active infection that may affect survival outcomes; (4) Patients with incomplete clinical or follow-up data.

High-throughput sequencing and differential expression analysis

Total RNA was extracted with TRIzol™ Reagent (Cat#15596026, Invitrogen, Waltham, MA, USA). The mRNA libraries were constructed and sequenced on a HiSeq 4000 platform (Cat#FC-410-1001, Illumina Inc., San Diego, CA, USA) by Gene Denovo Biotechnology Co., Ltd. (Guangzhou, China). Clean reads were aligned to the human reference genome, and gene-level counts were obtained. Differentially expressed genes were identified using standard pipelines (DESeq2) with predefined thresholds for fold-change and adjusted *p*-value (FDR), and expression values were transformed to $\log_2$ scale for visualization.

KEGG pathway enrichment and in silico prediction analyses

KEGG pathway enrichment analysis was performed on THAP7-AS1-upregulated genes using standard over-representation or gene set enrichment methods to identify invasion- and metastasis-related pathways. In silico prediction of IGF2BP3-RNA interactions along the full-length CCN2 transcript was conducted using established RBP-RNA binding prediction tools, with particular attention to high-scoring sites within the 3'UTR. Putative m^{6}A sites in CCN2 mRNA were predicted based on the DRACH consensus motif and dedicated m^{6}A prediction algorithms.

Bladder orthotopic xenograft model

All animal experiments were approved by the Institutional Animal Care and Use Committee (IACUC) of Fuzhou University Affiliated Provincial Hospital. Specific pathogen-free (SPF) grade female BALB/c nude mice were purchased from GemPharmatech Co., Ltd. (Nanjing, China, License No. SCXK 2020-0005). Mice were housed in a temperature-controlled (22 ± 2°C) and humidity-controlled (50 ± 5%) SPF facility with a 12-h light/12-h dark cycle, with free access to sterilized standard chow and water. A PerkinElmer IVIS Spectrum *in vivo* imaging system (Xenogen, Alameda, CA, USA) was used to monitor LN metastasis. Primary bladder tumors and pelvic lymph nodes were subsequently harvested and further analyzed. At the experimental endpoint (4 weeks after cell inoculation) or when mice met the humane endpoint criteria (e.g., tumor ulceration, body weight loss >20%, difficulty in urination, lethargy), mice were euthanized via intraperitoneal injection of an overdose of sodium pentobarbital (200 mg/kg). Death was confirmed by the permanent cessation of heartbeat and respiratory movement for at least 5 min, followed by verification of the absence of corneal and pedal withdrawal reflexes. This study was approved by the Animal Ethics Committee of Fuzhou University Affliated Provincial Hospital (IACUC-FPH-SL-202303160303).

Cell lines and cell culture

The human BCa cell line T24 was purchased from the American Type Culture Collection (ATCC, Cat#HTB-4, Manassas, VA, USA). Human lymphatic endothelial cells (HLECs) were obtained from ScienCell Research Laboratories (Cat#2500, Carlsbad, CA, USA). T24 cells were cultured in Roswell Park Memorial Institute (RPMI) 1640 medium (Cat#11875093, Invitrogen, Waltham, MA, USA). HLECs were cultured in endothelial cell medium (ECM; Cat#1001, ScienCell Research Laboratories). ECM was supplemented with 5% fetal bovine serum (FBS; Cat#0025, ScienCell Research Laboratories), and RPMI 1640 medium was supplemented with 10% FBS (Cat#10099-141, Gibco, Grand Island, NY, USA). All cells were cultured in a humidified 5% CO_2 incubator (Cat#3111, Thermo Fisher Scientific, Waltham, MA, USA) at 37°C. Cell line identity was authenticated by short tandem repeat (STR) DNA profiling via the AmpFLSTR Identifiler Kit (Cat#4322288, Thermo Fisher Scientific), and cells were routinely tested negative for mycoplasma contamination using the MycoAlert™ Mycoplasma Detection Kit (Cat#LT07-318, Lonza, Basel, Switzerland).

Plasmids, shRNAs/siRNAs, and transfection/infection

Full-length human THAP7-AS1 and CCN2 sequences were amplified from BCa cDNA and cloned into a lentiviral expression vector carrying a puromycin resistance cassette under the control of the CMV promoter to generate THAP7-AS1 and CCN2 overexpression constructs. The corresponding empty vector was used as a negative control. The sequences and detailed information of the siRNAs used in this study are provided in Supplementary Table 4. All constructs were verified by Sanger sequencing.

Short hairpin RNAs (shRNAs) targeting THAP7-AS1 and the corresponding non-targeting control shRNA (sh-NC) were cloned into a U6 promoter-driven lentiviral backbone. Small interfering RNAs (siRNAs) targeting IGF2BP3, METTL3 and CCN2, together with a non-targeting control siRNA (si-NC), were synthesized by Igebio (Guangzhou, China). The target sequences of shRNAs and siRNAs are listed in supplementary documents.

For transient knockdown experiments, BCa cells were transfected with siRNAs using a lipid-based transfection reagent according to the manufacturer's instructions. Unless otherwise indicated, functional and mechanistic assays were performed 48-72 h after transfection or after completion of antibiotic selection for stable lines. Knockdown and overexpression efficiencies were confirmed by qRT-PCR (and/or western blotting for protein-coding genes) prior to downstream analyses.

Protein extraction and western blotting analysis

Detailed information regarding the primary and secondary antibodies used in this study is provided in Supplementary Table 5. Anti-IGF2BP3: Rabbit monoclonal antibody, Cat#

ab177477, Abcam, Cambridge, UK; 1:1000 dilution. Anti-CCN2: Rabbit monoclonal antibody, Cat#ab209786, Abcam; 1:1000 dilution. Anti-GAPDH: Rabbit monoclonal antibody, Cat#5174, Cell Signaling Technology (CST), Danvers, MA, USA; 1:5000 dilution. HRP-conjugated goat anti-rabbit IgG secondary antibody: Cat#7074, CST; 1:5000 dilution.

ELISA

Levels of secreted CCN2 and TGFB3 in cell culture supernatants and tissue supernatants from BCa specimens were measured using commercial ELISA kits (Abcam) according to the manufacturer's instructions. Briefly, clarified supernatants were added to antibody-coated plates, incubated with detection antibody and substrate, and absorbance was read at the recommended wavelength. Protein concentrations were calculated from standard curves and normalized to cell number or tissue weight as appropriate.

RNA extraction and quantitative real-time PCR (qRT-PCR)

The resulting cDNA was analyzed by qRT-PCR to determine target gene expression on a Bio-Rad CFX96 system using TB Green II (Takara). The sequences of all primers used in this study are listed in Supplementary Table 4. Relative expression levels were calculated using the $2^{-\Delta CT}$ method, with GAPDH or ACTB as internal controls. The qRT-PCR reaction was performed in a 20 μL system containing: 10 μL TB Green II Premix Ex Taq (Takara), 0.4 μL forward primer (10 μM), 0.4 μL reverse primer (10 μM), 2 μL cDNA template, and 7.2 μL RNase-free ddH2O. The qRT-PCR reaction conditions were set as follows: initial denaturation at 95°C for 30 s; followed by 40 cycles of denaturation at 95°C for 5 s, annealing and extension at 60°C for 30 s; melting curve analysis was performed from 65°C to 95°C with 0.5°C increments per 5 s to verify amplification specificity.

Immunofluorescence staining

Sections were incubated with primary antibodies against IGF2BP3, CCN2, LYVE-1 and pan-cytokeratin at 4°C overnight, followed by fluorophore-conjugated secondary antibodies and DAPI counterstaining. Detailed information regarding the primary and secondary antibodies used in this study is provided in Supplementary Table 5. Images were acquired using FV3000 series confocal laser scanning microscope (Olympus, Hachioji-shi, Tokyo, Japan) with identical exposure settings across groups, and signal intensity or positive area was quantified using ImageJ-based analysis.

FISH

RNA FISH was performed to detect THAP7-AS1 in BCa cells and tissue sections using specific fluorescently labeled antisense probes. Briefly, cells or deparaffinized sections were fixed, permeabilized, hybridized with THAP7-AS1 probes, stringently washed, and counterstained with DAPI. Images were acquired with a confocal fluorescence microscope, and THAP7-AS1 signals were quantified using standardized exposure settings across groups.

For cell-based FISH analysis, cells seeded in confocal dishes were pretreated with 0.5% Triton X-100 to permeabilize the membranes, as described for the IF assays. Then, the THAP7-AS1 probes labeled with Alexa Fluor 594 (GenePharma, Shanghai, China) were used to hybridize the cells at 4°C overnight followed by the staining of cell nuclei with DAPI at room temperature for 10 min. The cells were examined under an FV3000 series confocal laser scanning microscope (Olympus, Hachioji-shi, Tokyo, Japan).

Subcellular fractionation

Subcellular fractionation was performed using a standard nuclear-cytoplasmic separation protocol. Briefly, BCa cells were lysed in a hypotonic buffer to obtain cytoplasmic fractions, and nuclear pellets were subsequently extracted in nuclear lysis buffer. RNA was isolated from each fraction and analyzed by qRT-PCR to determine THAP7-AS1 distribution, with GAPDH and U1 snRNA serving as cytoplasmic and nuclear controls, respectively.

Transwell invasion assay

BCa cells with the indicated genetic manipulations (such as THAP7-AS1 overexpression or knockdown) were seeded into the upper chamber in serum-free medium, and medium containing 10% FBS was added to the lower chamber as chemoattractant. After incubation, non-invading cells were removed, and invading cells on the lower membrane surface were fixed, stained and counted in multiple random fields.

Transendothelial migration assay

For transendothelial migration, human lymphatic endothelial cells (HLECs) were grown to confluence on Transwell inserts to form a monolayer. mCherry-labeled BCa cells with the indicated treatments were added to the upper chamber, and medium with 10% FBS was placed in the lower chamber. After incubation, cells that transmigrated to the underside of the insert were fixed, stained or directly imaged, and the number of mCherry-positive cells per field was quantified.

RNA pull-down and mass spectrometry

Biotin-labeled sense and antisense THAP7-AS1 transcripts were *in vitro* transcribed and incubated with lysates from BCa cells. RNA-protein complexes were captured using streptavidin beads, extensively washed, and eluted for analysis. Bound proteins were visualized by silver staining, and THAP7-AS1-enriched bands were excised and subjected to mass spectrometry to identify interacting proteins, followed by western blot validation of IGF2BP3 binding.

RNA immunoprecipitation (RIP) and m^{6}A-RIP-qRT-PCR

RIP was performed using an IGF2BP3-specific antibody or control IgG. Briefly, BCa cell lysates were incubated with antibody-coupled protein A/G beads, and RNA associated with immunoprecipitated complexes was extracted. Enrichment of THAP7-AS1 and CCN2 mRNA in IGF2BP3 IP versus IgG control was quantified by qRT-PCR and normalized to input to assess specific RNA-protein interactions under the indicated conditions.

For m^{6}A-RIP, total RNA was fragmented and incubated with an anti-m^{6}A antibody or control IgG immobilized on protein A/G beads. After washing, bound RNA was eluted, purified and subjected to qRT-PCR to measure CCN2 transcript enrichment in the m^{6}A fraction, and changes in CCN2 m^{6}A enrichment upon METTL3 knockdown were used to evaluate METTL3-dependent m^{6}A modification.

Actinomycin D chase assay

CCN2 mRNA stability was evaluated using actinomycin D chase assays. BCa cells with the indicated genetic manipulations were treated with actinomycin D to block transcription, and total RNA was collected at serial time points. CCN2 mRNA levels were quantified by qRT-PCR, normalized to baseline, and decay curves were fitted to calculate transcript half-life.

Patient-derived xenograft (PDX) model and in vivo THAP7-AS1 inhibition

Fresh BCa samples obtained from a patient who had undergone surgery at FZUAPH were implanted subcutaneously into immunodeficient mice to establish PDX models. Once tumors reached approximately 200 mm^3, mice were randomized to receive intratumoral injections of sh-THAP7-AS1 or sh-NC at defined intervals. All procedures, including injections and imaging, were performed under anesthesia with pentobarbital. At the experimental endpoint (36 days after the first injection), mice were euthanized using the same method described above, with death confirmed via the same criteria. Tumors were excised immediately after euthanasia for further analysis.

Public transcriptomic datasets and bioinformatic analysis

Publicly available transcriptomic datasets of human BCa were retrieved from the Gene Expression Omnibus (GEO; National Center for Biotechnology Information). The following cohorts were included in this study: GSE236932, GSE243441, GSE248167, GSE185901, GSE149582, GSE147983, GSE172359, GSE229410, GSE216037 and GSE212139. For each dataset, only primary BCa samples with available clinicopathological annotation and, where applicable, matched noncancerous adjacent tissues were included in the analyses.

All bioinformatic and statistical analyses of public datasets were performed in R (version 4.4.2; R Foundation for Statistical Computing, Vienna, Austria) using standard packages including limma, DESeq2, survival and survminer.

Statistical analysis

Data were analyzed using SPSS 26.0 (IBM). Unless otherwise indicated, experiments were repeated at least three times independently, and results are expressed as mean ± SD.

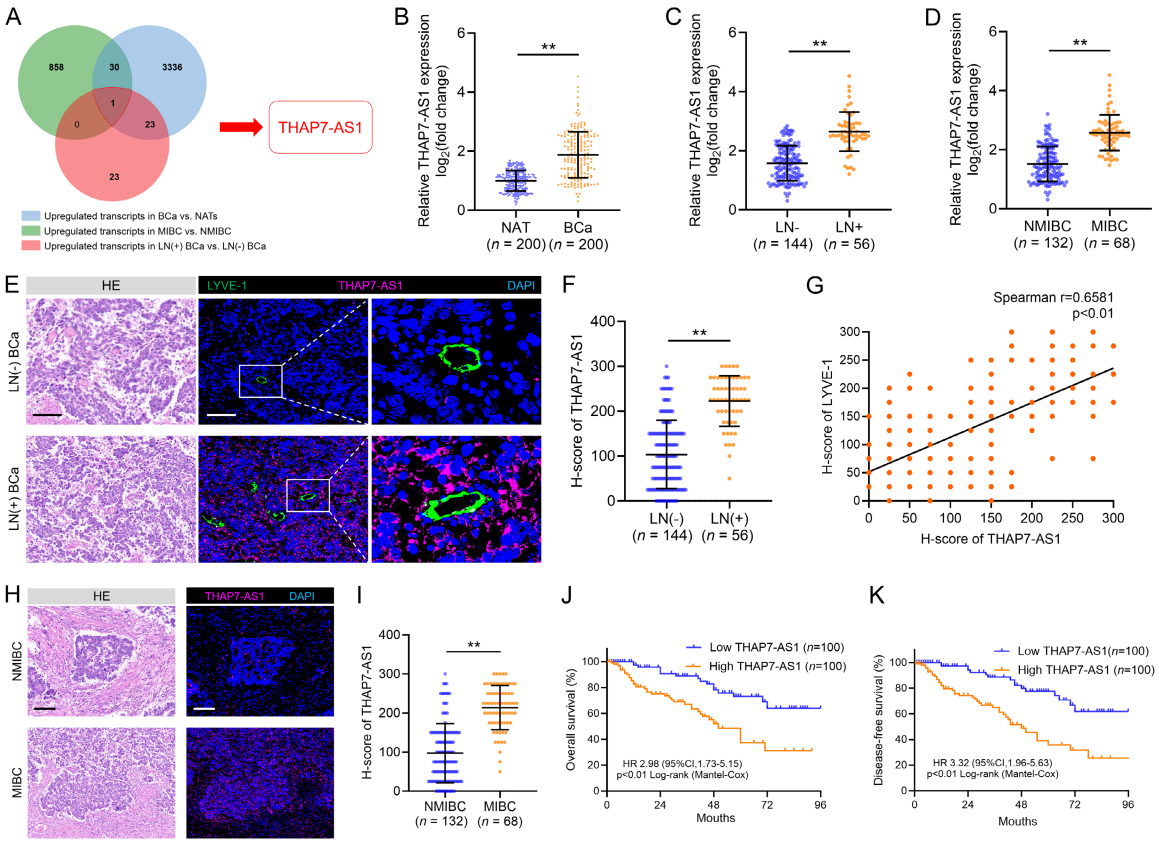

Figure 1. THAP7-AS1 Is Upregulated in Invasive and LN Metastatic BCa and Predicts Poor Prognosis. (A) The identification and characterization of THAP7-AS1 in BCa. (B) qRT-PCR analysis for the THAP7-AS1 expression in BCa tissues (n = 200) paired with NATs (n = 200). Error bars show the mean ± SD; ns, not significant and **P < 0.01 by nonparametric Mann-Whitney *U* test. (C) qRT-PCR analysis of the THAP7-AS1 expression in 200 BCa tissues with respect to LN status. Error bars show the mean ± SD; ns, not significant and **P < 0.01 by nonparametric Mann-Whitney *U* test. (D) qRT-PCR analysis for the THAP7-AS1 expression in MIBC (n = 68) with NMIBC (n = 132). Error bars show the mean ± SD; ns, not significant and **P < 0.01 by nonparametric Mann-Whitney *U* test. (E, F) Representative fluorescence images and quantification for THAP7-AS1 expression in BCa tissues with or without LN metastasis. Scale bar, 50 μm (magnification ×300). (G) Correlation analysis between THAP7-AS1 expression and LYVE-1 expression in the BCa tissues. (H, I) Representative fluorescence images and quantification for THAP7-AS1 expression in MIBC and NMIBC. Scale bar, 50 μm (magnification ×300). (J, K) Kaplan-Meier survival analysis of the OS (J) and DFS (K) of patients with BCa with low versus high THAP7-AS1 expression. The cutoff value is the median.

Student's t test or Mann-Whitney U test was used for two-group comparisons, paired t test for matched tumor and adjacent tissues, and one-way ANOVA with Dunnett's test for multiple groups. Repeated measures ANOVA was used for comparisons among multiple groups with repeated measurements. Categorical variables were presented as frequencies (n) and percentages (%), and group comparisons were performed using the χ^2 test. Survival outcomes were analyzed by Kaplan-Meier and log-rank tests, and prognostic factors were assessed using Cox regression models. P < 0.05 was considered significant.

Results

THAP7-AS1 is upregulated in invasive and LN metastatic BCa and predicts poor prognosis

To identify key transcripts that contribute to BCa progression, we first interrogated multiple independent transcriptomic datasets from the Gene Expression Omnibus (GEO). Across all analyzed cohorts, THAP7-AS1 expression was consistently higher in BCa tissues than in normal urothelium and was further increased in muscle-invasive compared with non-muscle-invasive tumors, as well as in LN metastatic

versus non-metastatic cases where nodal status was available (**Figure 1A**). Analysis of our institutional cohort by qRT-PCR and in situ hybridization corroborated these observations, showing significantly elevated THAP7-AS1 levels in invasive and LN-positive tumors relative to matched adjacent non-tumor tissues (**Figure 1B-D**). THAP7-AS1 expression was markedly elevated in LN metastatic tumors compared with non-metastatic tumors, and THAP7-AS1 levels positively correlated with the density of lymphangiogenic markers in corresponding specimens (**Figure 1E-G**). Consistently, the staining intensity of THAP7-AS1 was significantly higher in muscle-invasive than in non-muscle-invasive BCa tissues, supporting an association between THAP7-AS1 upregulation, lymphangiogenesis and aggressive disease behavior (**Figure 1H**, **1I**). High THAP7-AS1 expression was positively associated with adverse clinicopathological features, including higher T stage, poor differentiation and nodal involvement (Supplementary Table 1). In our validation cohort, patients with THAP7-AS1-high tumors had significantly shorter overall and disease-free survival than those with THAP7-AS1-low tumors, and THAP7-AS1 remained an independent predictor of poor outcome in multivariate Cox regression after adjustment for established prognostic variables (**Figure 1J**, **1K** and Supplementary Tables 2, 3). Together, these data demonstrate that THAP7-AS1 is upregulated in invasive and LN-metastatic BCa and is associated with poor prognosis.

THAP7-AS1 enhances invasion and transendothelial migration of BCa cells in vitro

To determine whether THAP7-AS1 directly modulates the invasive behavior of BCa cells, we performed functional assays in representative BCa cell lines. Stable THAP7-AS1 overexpression and knockdown in the indicated BCa cells were confirmed by qRT-PCR (Supplementary Figure 1A, 1C). THAP7-AS1 modulation did not produce overt effects on short-term cell viability or proliferation, excluding gross growth differences as a major confounder. In Matrigel invasion assays, THAP7-AS1 overexpression increased the number of invading cells, whereas THAP7-AS1 knockdown substantially reduced invasive capacity (**Figure 2A**, **2C**). To model lymphovascular dissemination, we next examined tumor cell transmigration across lymphatic endothelial monolayers using a transendothelial Transwell system. THAP7-AS1-overexpressing BCa cells exhibited significantly enhanced transendothelial migration compared with control cells, whereas THAP7-AS1 silencing robustly impaired their ability to traverse the endothelial barrier (**Figure 2B**, **2D**). These effects were reproducible across independent clones and cell lines and were accompanied by concordant changes in invasive morphology. Collectively, these data demonstrate that THAP7-AS1 potently promotes invasion and transendothelial migration of BCa cells *in vitro*, functionally linking elevated THAP7-AS1 expression to a pro-invasive, lymphovascular transmigratory phenotype.

THAP7-AS1 drives lymphatic metastasis of BCa in vivo

Given that THAP7-AS1 enhanced invasion and transendothelial migration *in vitro*, we next asked whether it is sufficient to drive lymphatic dissemination *in vivo*. BCa cells were engineered to stably overexpress THAP7-AS1 or carry empty vector and implanted into immunodeficient mice to establish xenografts. Primary tumor growth was comparable between groups at endpoint, excluding gross differences in tumor burden as a major confounder. THAP7-AS1 overexpression markedly increased LN metastasis, as evidenced by a higher incidence of metastatic draining LNs per mouse (**Figure 2E-G**). Immunostaining showed markedly increased LYVE-1-positive lymphatic vessels in bladder tumors from the THAP7-AS1-overexpressing group, consistent with enhanced lymphangiogenesis in association with increased lymphatic metastasis (**Figure 2H-J**). Collectively, these *in vivo* data demonstrate that enforced THAP7-AS1 expression is sufficient to drive lymphatic metastasis of BCa.

THAP7-AS1 serves as a molecular scaffold bridging IGF2BP3 and CCN2 mRNA

We first sought to identify RNA-binding proteins that interact with THAP7-AS1 and might mediate its pro-invasive function. RNA pulldown coupled with mass spectrometry revealed IGF2BP3 as one of the most prominently enriched THAP7-AS1-associated proteins (**Figure 3A**, **3B**). This interaction was confirmed by RNA pulldown followed by immunoblotting, which showed robust recruitment of endogenous

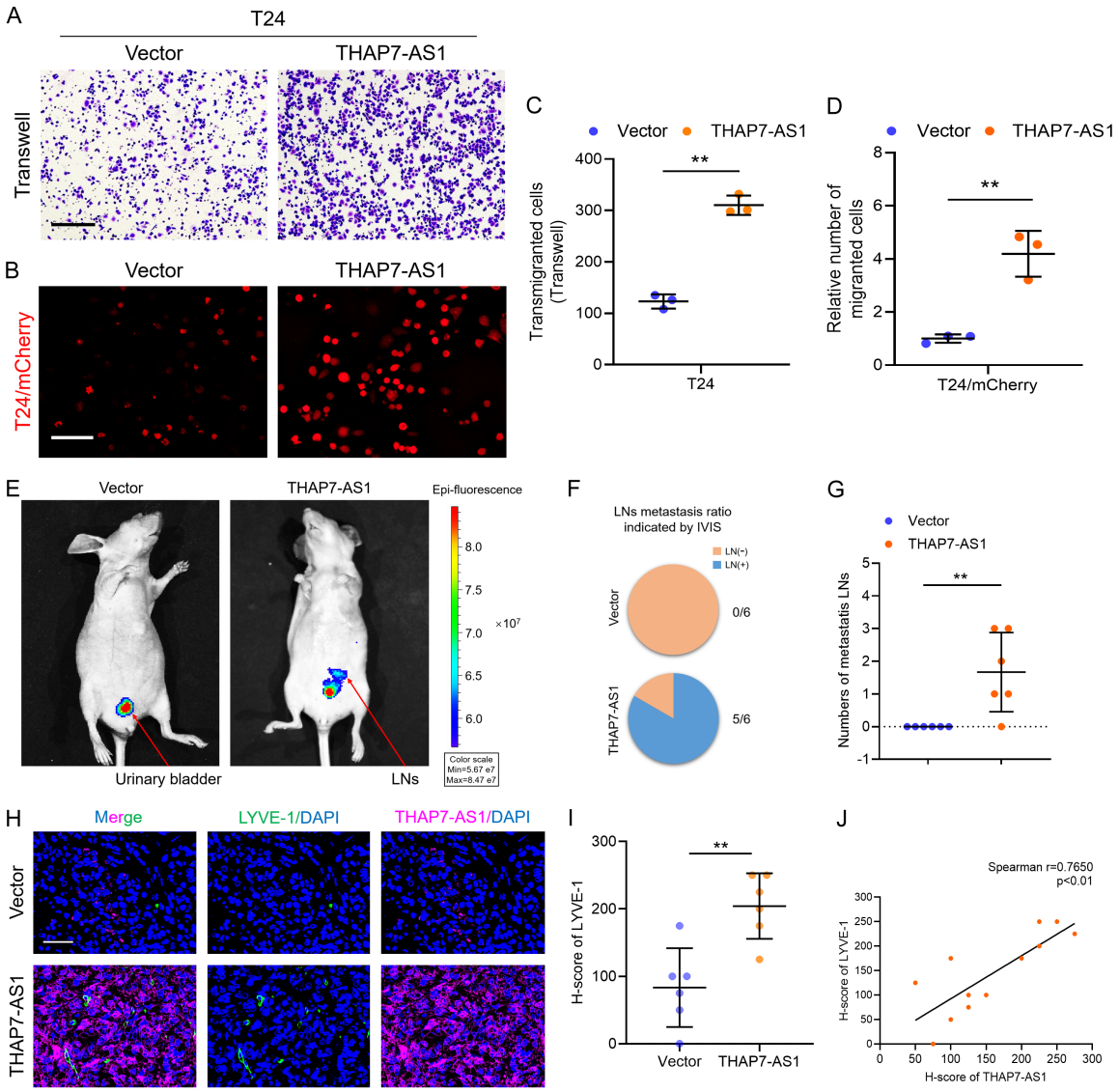

Figure 2. THAP7-AS1 promotes invasion, transendothelial migration, and LN metastasis of BCa *in vitro* and *in vivo*. A. Representative images of BCa cells invading across Matrigel-coated matrices in Transwell assays. Scale bar, 100 μm (magnification ×150). B. Representative images of mCherry-labeled BCa cells transmigrating across monolayers of HLECs in transendothelial migration assays. Scale bar, 100 μm (magnification ×150). C. Quantification of BCa cells invading across Matrigel-coated matrices in Transwell assays. Error bars show the mean ± SD, **P < 0.01 by nonparametric Mann-Whitney *U* test. D. Quantification of mCherry-labeled BCa cells transmigrating across monolayers of HLECs in transendothelial migration assays. Error bars show the mean ± SD, **P < 0.01 by nonparametric Mann-Whitney *U* test. E. Representative bioluminescence images of nude mice treated with T24 cells transfected with the indicated constructs (n = 6). The red arrows indicate primary tumor and metastatic LNs. F. Pie charts showing the percentages of mice with LN metastasis in each group. G. Quantification of the metastatic number of pelvic LNs in mice from indicated groups. Error bars show the mean ± SD, **P < 0.01 by nonparametric Mann-Whitney *U* test. H. Representative fluorescence images showing LYVE-1 expression and THAP7-AS1 expression in bladder tumors from mice in the indicated groups. Scale bar, 50 μm (magnification ×300). I. Quantification of LYVE-1 expression in urinary bladder tumors from mice in the indicated groups. Error bars show the mean ± SD, **P < 0.01 by nonparametric Mann-Whitney *U* test. J. Correlation analysis between THAP7-AS1 expression and LYVE-1 expression in bladder tumors from mice in the indicated groups.

IGF2BP3 by THAP7-AS1 but not by antisense RNA, and by IGF2BP3 RIP demonstrating significant enrichment of THAP7-AS1 in IGF2BP3 complexes compared with IgG controls (**Figure 3C**, **3D**). Consistent with a role in aggressive disease, IGF2BP3 protein was markedly upregulated in invasive and LN-positive BCa tissues in our cohort, and its expression positively cor-

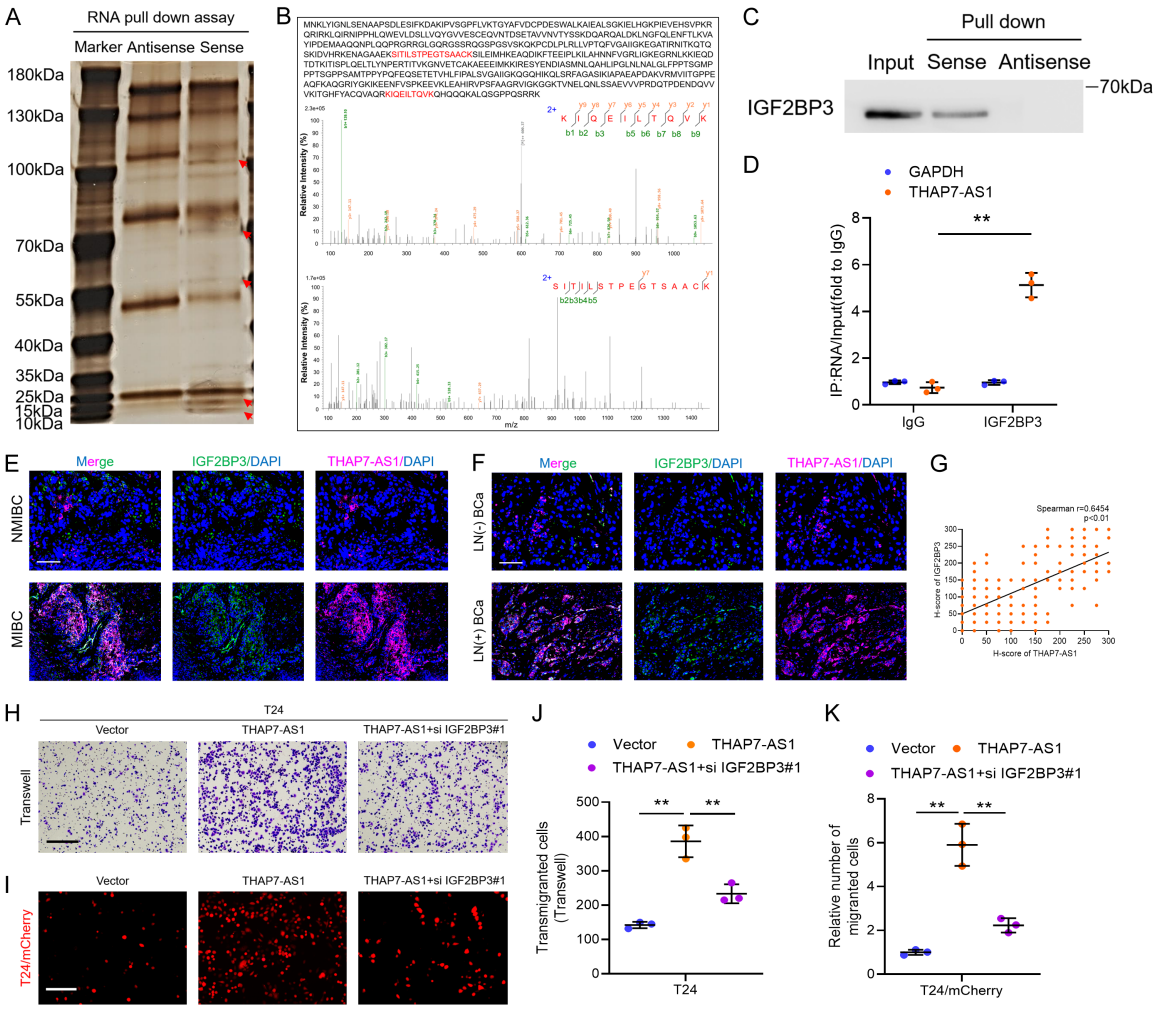

Figure 3. THAP7-AS1 interacts with IGF2BP3 and requires this interaction to promote invasion. (A, B) Silver staining of proteins from RNA pull-down assays using biotin-labeled THAP7-AS1 sense and antisense probes in BCa cells (A). The THAP7-AS1-enriched band indicated by silver staining was subjected to mass spectrometry (MS) analysis (B). (C) Western blotting analysis after RNA pull-down assays with whole-cell lysate. (D) RIP assays of IGF2BP3 in T24 cells showing enrichment of THAP7-AS1. Error bars show the mean ± SD, **P < 0.01 by two-tailed Student's *t* test. (E) Representative fluorescence images of IGF2BP3 expression and THAP7-AS1 expression in BCa tissues with or without LN metastasis. Scale bar, 50 μm (magnification ×300). (F) Representative fluorescence images of IGF2BP3 expression and THAP7-AS1 expression in NMIBC or MIBC. Scale bar, 50 μm (magnification ×300). (G) Correlation analysis between THAP7-AS1 expression and IGF2BP3 expression in BCa tissues from clinical cohorts. (H) Representative images of BCa cells invading across Matrigel-coated matrices in Transwell assays. Scale bar, 100 μm (magnification ×150). (I) Representative images of mCherry-labeled BCa cells transmigrating across monolayers of HLECs in transendothelial migration assays. Scale bar, 100 μm (magnification ×150). (J) Quantification of BCa cells invading across Matrigel-coated matrices in Transwell assays. Error bars show the mean ± SD, **P < 0.01 by one-way ANOVA followed by Dunnett's tests. (K) Quantification of mCherry-labeled BCa cells transmigrating across monolayers of HLECs in transendothelial migration assays. Error bars show the mean ± SD, **P < 0.01 by one-way ANOVA followed by Dunnett's tests.

related with THAP7-AS1 levels (**Figure 3E-G**). Functionally, IGF2BP3 knockdown largely abrogated the increase in invasion and transendothelial migration induced by THAP7-AS1 overexpression (**Figure 3H-K** and Supplementary Figure 1B). Collectively, these data identify IGF2BP3 as a direct THAP7-AS1-binding RNA-binding protein and a critical mediator of THAP7-AS1-driven invasive behavior in BCa.

THAP7-AS1-IGF2BP3-m^{6}A axis post-transcriptionally stabilizes CCN2 mRNA

To identify downstream effectors of the THAP7-AS1-IGF2BP3 axis, we integrated RNA-seq fol-

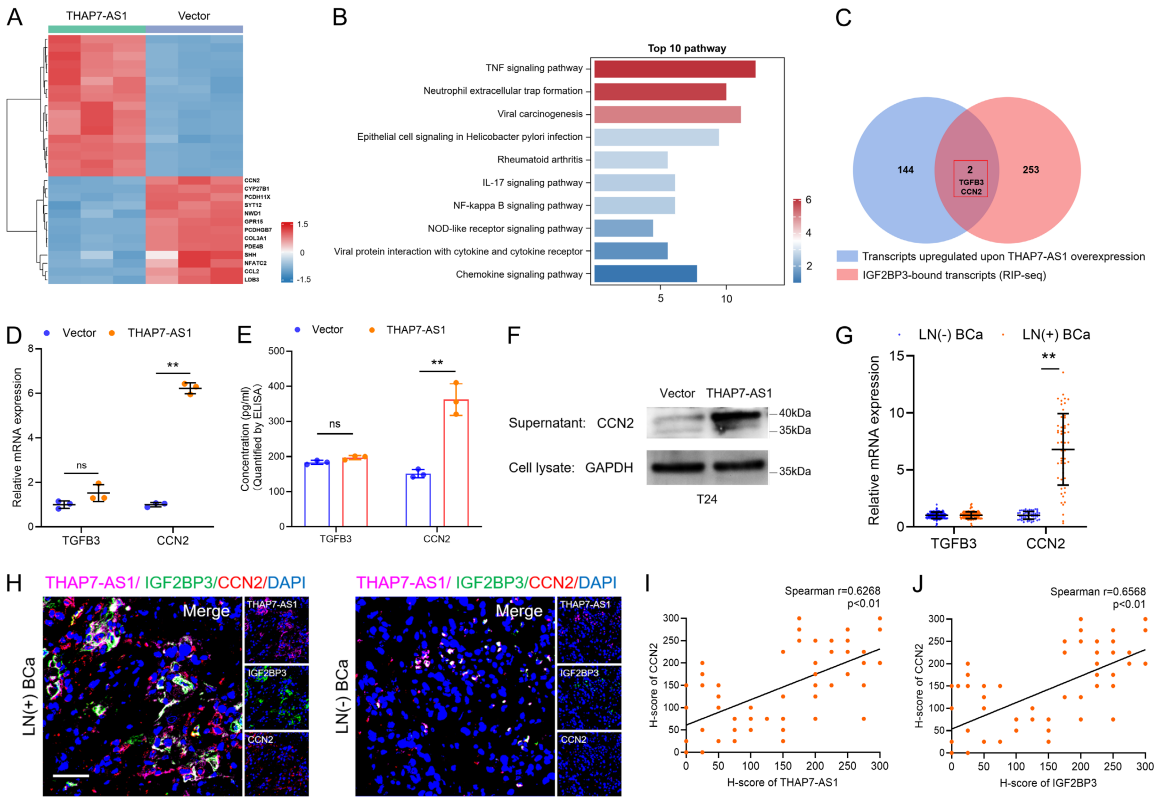

Figure 4. THAP7-AS1–IGF2BP3 axis upregulates the secreted effector CCN2 and associates with lymph node metastasis in BCa. A. Heatmap of differentially expressed genes in THAP7-AS1-overexpressing BCa cells versus control cells based on RNA-seq analysis. B. KEGG pathway enrichment analysis of THAP7-AS1-induced differentially expressed genes, shown as a bar plot of the top invasion- and metastasis-related pathways. C. Workflow for identifying upregulated genes in THAP7-AS1-overexpressing BCa cells. D. qRT-PCR analysis of the indicated mRNA expression in THAP7-AS1-overexpressing BCa cells. Error bars show the mean ± SD; ns, not significant; **P < 0.01 by two-tailed Student's *t* test. E. Quantification of the indicated protein levels in THAP7-AS1-overexpressing BCa cells by ELISA. Error bars show the mean ± SD; ns, not significant; **P < 0.01 by two-tailed Student's *t* test. F. Western blotting analysis of CCN2 in cell culture supernatants from THAP7-AS1-overexpressing BCa cells. G. Quantification of the indicated protein levels in tissue supernatants from BCa specimens with or without LN metastasis by ELISA. Error bars show the mean ± SD; ns, not significant; **P < 0.01 by two-tailed Student's *t* test. H. Representative fluorescence images of IGF2BP3, CCN2 and THAP7-AS1 expression in BCa tissues with or without LN metastasis. Scale bar, 50 μm (magnification ×300). I. Correlation analysis between THAP7-AS1 and CCN2 expression in BCa tissues from the clinical cohort. J. Correlation analysis between IGF2BP3 and CCN2 expression in BCa tissues from the clinical cohort.

lowing THAP7-AS1 overexpression with available IGF2BP3-binding datasets. RNA-seq of BCa cells with THAP7-AS1 overexpression identified a set of genes consistently induced by THAP7-AS1 (**Figure 4A**, **4B**). Intersection of these THAP7-AS1-upregulated transcripts with IGF2BP3-bound targets defined by RIP datasets yielded two secreted factors, TGFB3 and CCN2, as candidate effectors (**Figure 4C**). Among them, CCN2 exhibited the most robust and concordant induction at the mRNA level (**Figure 4D**). THAP7-AS1 overexpression increased CCN2 mRNA abundance, intracellular CCN2 protein and secreted CCN2 in conditioned media, as detected by qRT-PCR, immunoblotting and ELISA (**Figure 4D-F**). In clinical specimens, CCN2 levels were higher in LN-positive than in LN-negative tumors and correlated positively with THAP7-AS1 and IGF2BP3 expression (**Figure 4G-J**). Collectively, these data identify CCN2 as a major downstream effector linked to the THAP7-AS1-IGF2BP3 axis and lymphatic dissemination in BCa.

RNA FISH combined with nuclear-cytoplasmic fractionation showed that THAP7-AS1 is predominantly localized in the cytoplasm of BCa cells, suggesting a post-transcriptional mode

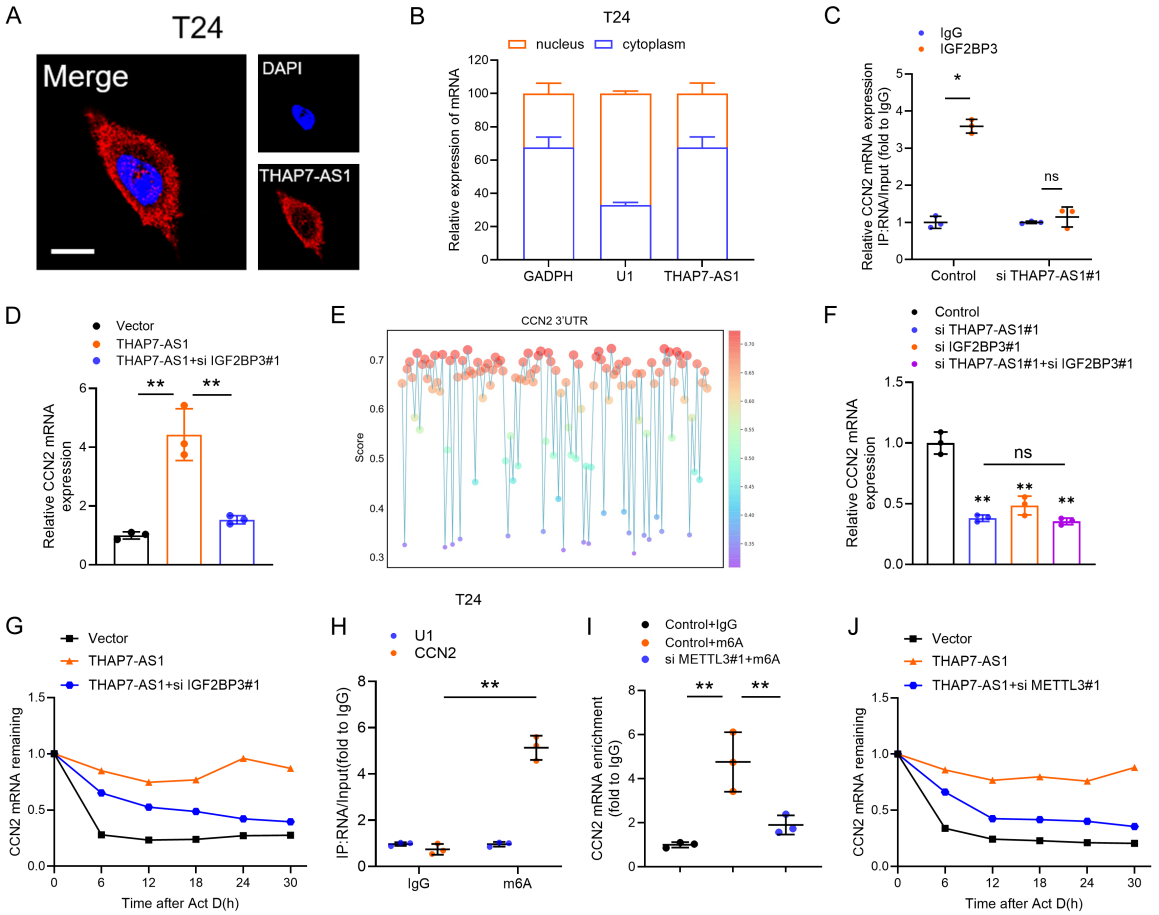

Figure 5. THAP7-AS1-IGF2BP3-m^{6}A axis post-transcriptionally stabilizes CCN2 mRNA in BCa cells. A. Confocal images showing the intracellular localization of THAP7-AS1 in BCa cells. Scale bar, 5 μm (magnification ×1600). B. Subcellular fractionation-qRT-PCR analysis showing predominant cytoplasmic localization of THAP7-AS1 in BCa cells, with GAPDH as a cytoplasmic control. C. IGF2BP3 RIP-qRT-PCR analysis in BCa cells showing enrichment of CCN2 mRNA. Error bars show the mean ± SD, **P < 0.01 by two-tailed Student's *t* test. D. qRT-PCR analysis of CCN2 mRNA expression in BCa cells under the indicated treatments. Error bars show the mean ± SD, **P < 0.01 by one-way ANOVA followed by Dunnett's tests. E. Predicted IGF2BP3 binding score profile across the CCN2 transcript, highlighting a prominent cluster of high-scoring binding sites within the 3'UTR. F. qRT-PCR analysis of CCN2 mRNA expression in BCa cells under the indicated treatments. Error bars show the mean ± SD, **P < 0.01 by one-way ANOVA followed by Dunnett's tests. G. Assessment of CCN2 mRNA stability in BCa cells under the indicated treatments. Error bars show the mean ± SD, **P < 0.01 by one-way ANOVA followed by Dunnett's tests. H. m^{6}A-RIP-qRT-PCR analysis in BCa cells showing enrichment of CCN2 mRNA. Error bars show the mean ± SD, **P < 0.01 by two-tailed Student's *t* test. I. m^{6}A-RIP-qRT-PCR analysis of CCN2 mRNA in BCa cells under the indicated treatments. Error bars show the mean ± SD, **P < 0.01 by one-way ANOVA followed by Dunnett's tests. J. Assessment of CCN2 mRNA stability in BCa cells under the indicated treatments. Error bars show the mean ± SD, **P < 0.01 by one-way ANOVA followed by Dunnett's.

of action (**Figure 5A**, **5B**). Given the identification of CCN2 as a downstream effector of the THAP7-AS1-IGF2BP3 axis, we next asked whether THAP7-AS1 regulates CCN2 expression by facilitating IGF2BP3-dependent stabilization of CCN2 transcripts. IGF2BP3 RIP-qPCR confirmed robust enrichment of CCN2 mRNA in IGF2BP3 complexes under basal conditions, whereas THAP7-AS1 knockdown significantly reduced CCN2 recovery, indicating that THAP7-AS1 promotes IGF2BP3–CCN2 complex formation (**Figure 5C**). Consistently, IGF2BP3 silencing decreased CCN2 mRNA levels (**Figure 5D**). To further support CCN2 as a direct post-transcriptional target of IGF2BP3, in silico IGF2BP3-RNA binding prediction applied to the full-length CCN2 transcript revealed a pronounced cluster of high-scoring binding sites within the 3'UTR,

whereas predicted binding scores across the 5'UTR and coding region were comparatively low (**Figure 5E**). Using the canonical DRACH m^{6}A modification motif, we identified three high-confidence putative m^{6}A sites within this IGF2BP3-binding cluster, with the highest-confidence core site being the GGACA motif at chr1:8297745 (GRCh38/hg38), which is the predicted m^{6}A site recognized by IGF2BP3 to mediate CCN2 mRNA stabilization. THAP7-AS1 or IGF2BP3 knockdown each reduced CCN2 expression, and combined THAP7-AS1 and IGF2BP3 inhibition did not further suppress CCN2 beyond IGF2BP3 knockdown alone, placing CCN2 downstream of a THAP7-AS1-IGF2BP3 module (**Figure 5F** and Supplementary Figure 1C).

Given that the predominant cytoplasmic localization of THAP7-AS1 together with its ability to bridge IGF2BP3 and CCN2 mRNA suggested a role in post-transcriptional control of CCN2 stability, we evaluated CCN2 transcript turnover using actinomycin D chase assays. THAP7-AS1 overexpression significantly prolonged the half-life of CCN2 mRNA compared with vector control, whereas concomitant IGF2BP3 knockdown abrogated this effect, indicating that THAP7-AS1 stabilizes CCN2 transcripts in an IGF2BP3-dependent manner (**Figure 5G**). Given that IGF2BP3 is a canonical m^{6}A reader, we next examined whether CCN2 mRNA carries METTL3-dependent m^{6}A marks. m^{6}A-RIP-qPCR demonstrated strong enrichment of CCN2 transcripts in m^{6}A immunoprecipitates relative to IgG, and METTL3 knockdown reduced CCN2 recovery in the m^{6}A-IP fraction (**Figure 5H** and Supplementary Figure 1D). Consistently, METTL3 depletion phenocopied IGF2BP3 knockdown in actinomycin D chase assays and prevented THAP7-AS1 from prolonging CCN2 mRNA half-life (**Figure 5I**, **5J**). Collectively, these data demonstrate that cytoplasmic THAP7-AS1 enforces post-transcriptional stabilization of CCN2 mRNA by engaging an IGF2BP3-m^{6}A axis.

THAP7-AS1-IGF2BP3-CCN2 axis mediates invasion and lymphatic metastasis and associates with adverse clinical outcome

Functionally, we next evaluated whether the THAP7-AS1-IGF2BP3-CCN2 axis mediates the invasive and lymphatic metastatic phenotypes driven by THAP7-AS1. Enforced THAP7-AS1 expression increased Matrigel invasion and transendothelial migration, whereas concomitant CCN2 knockdown largely abrogated these pro-invasive and pro-transendothelial effects (**Figure 6A**, **6B** and Supplementary Figure 1E). Re-expression of CCN2 significantly rescued the impairment of invasion and transendothelial migration induced by THAP7-AS1 knockdown, though the rescue effect was partial (**Figure 6C**), suggesting that additional downstream effectors may be involved in THAP7-AS1-mediated pro-metastatic function. *In vivo*, THAP7-AS1 overexpression significantly increased LN metastatic burden, as reflected by a higher number of metastatic draining LNs per mouse and a marked increase in pan-cytokeratin-positive tumor infiltration within the nodes (**Figure 6D**, **6E**). Importantly, IGF2BP3 or CCN2 knockdown in THAP7-AS1-overexpressing cells reduced both the frequency of LN metastasis and the extent of nodal pan-cytokeratin infiltration, indicating that IGF2BP3 and CCN2 are required for THAP7-AS1-driven lymphatic dissemination *in vivo* (**Figure 6D**, **6E**).

Preclinical and clinical evidence that the THAP7-AS1-IGF2BP3-CCN2 axis associates with adverse clinical outcome

Since THAP7-AS1 plays a crucial role in bladder cancer LN metastasis, we further established PDX models using tumor tissues from patients with LN metastatic bladder cancer to determine the therapeutic effect of THAP7-AS1 inhibition. When PDX tumors reached 200 mm^3, the mice were randomly divided into two groups and intratumorally injected with sh-THAP7-AS1 or sh-NC. The results showed that treatment with sh-THAP7-AS1 significantly suppressed the growth of tumor volume in PDX models compared with the controls (**Figure 6F**). Moreover, FISH for THAP7-AS1 combined with immunofluorescence for CCN2 in PDX tumors revealed that THAP7-AS1 silencing in PDX tumors markedly reduced CCN2 expression compared with the control group (**Figure 6G**). Collectively, these results demonstrate that targeting THAP7-AS1 might serve as a potential treatment for LN-metastatic bladder cancer.

Clinically, analysis of our institutional cohort showed that tumors with high THAP7-AS1 expression exhibited increased CCN2 levels (**Figure 4H**). qRT-PCR and immunofluorescence consistently revealed higher CCN2 expression

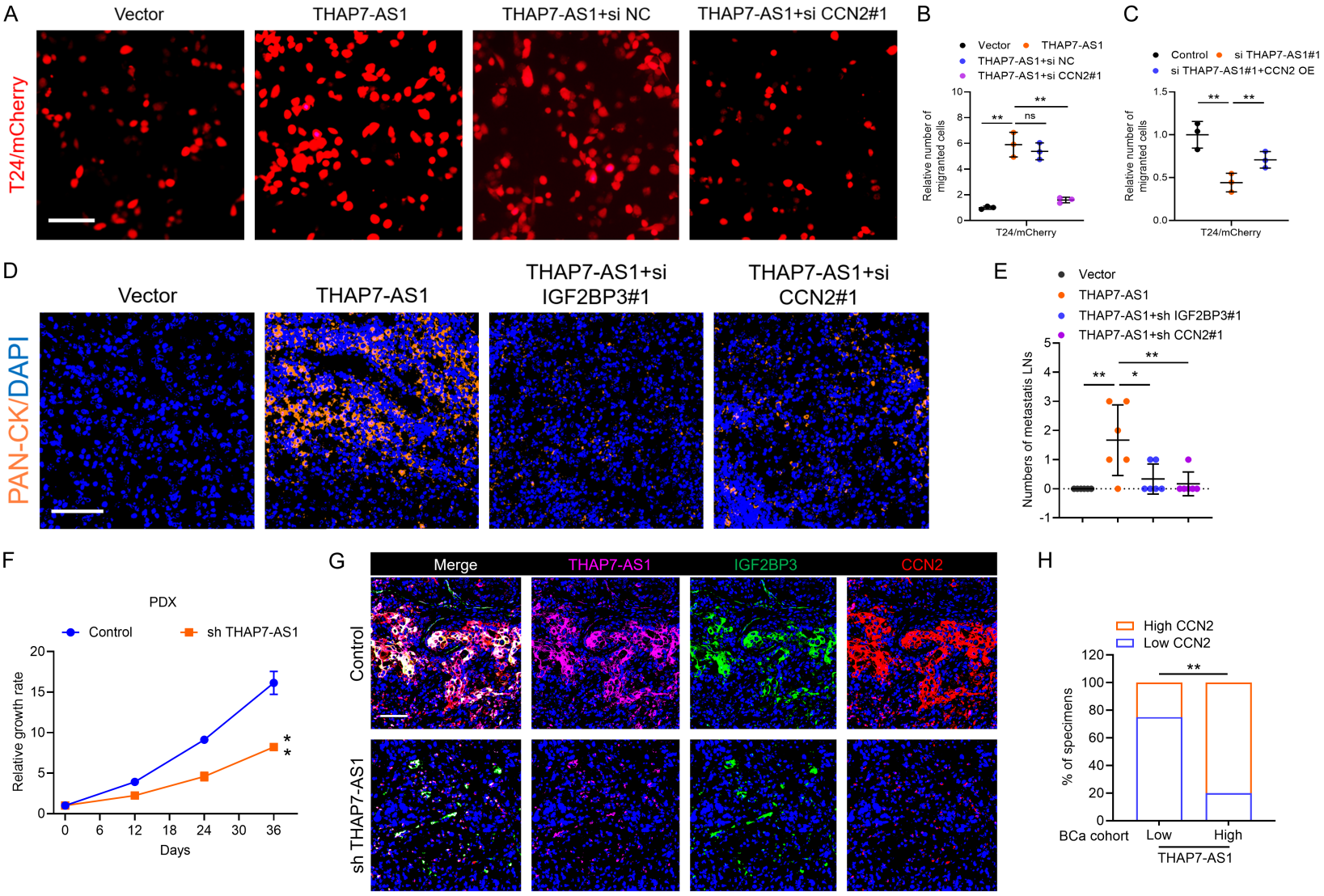

Figure 6. THAP7-AS1-IGF2BP3-CCN2 axis promotes transendothelial migration and lymphatic metastasis in vivo and associates with clinical THAP7-AS1-CCN2 co-expression. A. Representative images of mCherry-labeled BCa cells transmigrating across monolayers of HLECs in transendothelial migration assays. Scale bar, 100 μm (magnification ×150). B, C. Quantification of mCherry-labeled BCa cells transmigrating across monolayers of HLECs in transendothelial migration assays. Error bars show the mean ± SD; ns, not significant; **P < 0.01 by one-way ANOVA followed by Dunnett's tests. D. Representative fluorescence images showing pan-cytokeratin-positive tumor cell infiltration in pelvic LNs from indicated groups. Scale bar, 50 μm (magnification ×300). E. Quantification of the number of metastatic

pelvic LNs in mice from indicated groups. Error bars show the mean ± SD, *P < 0.05 and **P < 0.01 by one-way ANOVA followed by Dunnett's tests. F. Relative tumor growth curves of mice bearing control or THAP7-AS1 knockdown tumors (n = 6). Error bars show the mean ± SD, **P < 0.01 by two-tailed Student's *t* test. G. Representative fluorescence images of IGF2BP3, CCN2 expression and THAP7-AS1 expression in PDX tumor tissues. Scale bar, 50 μm (magnification ×300). H. Association between THAP7-AS1 and CCN2 expression status in BCa tissues from the clinical cohort. **P < 0.01 by the χ^2 test.

in THAP7-AS1-high tumors compared with THAP7-AS1-low tumors, and THAP7-AS1 and CCN2 levels were positively correlated in paired specimens (**Figures 4I** and **6H**). These data support CCN2 as a clinically relevant effector associated with THAP7-AS1 activation in BCa.

Discussion

Lymphatic metastasis is a key determinant of stage, treatment choice and outcome in BCa, yet the RNA-centered circuits that endow tumor cells with lymphatic metastatic competence remain poorly defined [19-21]. LncRNAs and epitranscriptomic m^{6}A modifications have emerged as central regulators of malignant progression, in part by reprogramming post-transcriptional control of metastasis-related transcripts [7, 22, 23]. Here, we identify THAP7-AS1 as a lncRNA upregulated in invasive and LN-positive BCa, closely associated with adverse clinicopathological features and poor prognosis, and functionally required for invasion, transendothelial migration and lymphatic dissemination. Our data indicate that cytoplasmic THAP7-AS1 assembles an IGF2BP3-m^{6}A-CCN2 ribonucleoprotein complex, which selectively stabilizes CCN2 mRNA and thereby sustains a pro-invasive, lymphotropic transcriptional state.

Mechanistically, this study defines THAP7-AS1 as a molecular scaffold that connects a canonical m^{6}A reader to a discrete effector transcript in BCa. RNA-binding protein (RBP) interactomes in cancer have revealed that scaffold lncRNAs frequently serve as organizing hubs that tether RBPs to specific RNA substrates and thereby impose specificity on post-transcriptional regulation [5, 22, 24]. In line with this paradigm, RNA pulldown and mass spectrometry identify IGF2BP3 as a dominant THAP7-AS1-interacting RBP, and IGF2BP3 RIP demonstrates that THAP7-AS1 and CCN2 mRNA coexist within IGF2BP3-containing complexes. THAP7-AS1 depletion diminishes IGF2BP3-bound CCN2 without altering IGF2BP3 expression, and combined THAP7-AS1 and IGF2BP3 inhibition does not further suppress CCN2 beyond IGF2BP3 knockdown alone, placing CCN2 downstream of a THAP7-AS1-IGF2BP3 module. Given that IGF2BP family proteins act as m^{6}A readers that enhance the stability of m^{6}A-decorated oncogenic transcripts, our demonstration that CCN2 transcripts bear METTL3-dependent m^{6}A modifications and are stabilized by THAP7-AS1 in an IGF2BP3- and m^{6}A-dependent manner provides mechanistic linkage between lncRNA scaffolding, m^{6}A recognition and effector mRNA persistence [9, 25, 26]. While our RNA pull-down and RIP assays confirm a specific and robust interaction between THAP7-AS1 and IGF2BP3, further cell-free biochemical assays are required to definitively verify whether this interaction is direct or mediated by auxiliary protein partners.

Functionally and clinically, our data point to CCN2 as a key effector through which THAP7-AS1-IGF2BP3 signaling promotes invasion and lymphatic spread. CCN2 has been implicated as a multi-faceted mediator of tumor cell motility, matrix remodeling and metastatic niche formation across several malignancies, and its overexpression correlates with LN metastasis and poor outcome in clinical cohorts. In BCa cells, THAP7-AS1 overexpression increases CCN2 at the mRNA, intracellular protein and secreted levels, whereas IGF2BP3 or CCN2 knockdown largely abrogates THAP7-AS1-driven Matrigel invasion and transendothelial migration [27-29]. *In vivo*, THAP7-AS1 overexpression selectively augments LN metastatic burden and nodal pan-cytokeratin infiltration without substantially altering primary tumor growth, and these effects are reversed by IGF2BP3 or CCN2 depletion. In patient specimens, CCN2 expression positively correlates with THAP7-AS1 and IGF2BP3 levels, supporting activation of this axis in clinically aggressive disease. Together, these findings argue that THAP7-AS1 promotes lymphatic dissemination not merely as a correlate of high-grade biology but by enforcing an IGF2BP3-m^{6}A-CCN2 regulatory program that integrates intrinsic post-tran-

scriptional rewiring with extrinsic microenvironmental modulation. Notably, CCN2 re-expression only partially rescued the invasive and metastatic phenotypes caused by THAP7-AS1 silencing, indicating that CCN2 is a key but not the sole downstream effector of the THAP7-AS1-IGF2BP3 axis. Our RNA-seq analysis identified TGFB3 as another candidate target of this axis, and other m^{6}A-modified transcripts involved in tumor invasion, matrix remodeling, and lymphangiogenesis may also serve as downstream effectors, which will be systematically characterized in our future studies.

Several limitations of this study should be acknowledged. First, our study was based on a single-center clinical cohort, and the prognostic value of THAP7-AS1 needs to be further validated in large-scale, multi-center cohorts. Second, while we identified CCN2 as a key downstream effector of the THAP7-AS1-IGF2BP3 axis, the partial rescue effect of CCN2 re-expression indicates that other downstream targets may also contribute to THAP7-AS1-mediated lymphatic metastasis, which requires further systematic exploration. Third, our in vivo functional experiments were performed in immunodeficient mouse models, which cannot fully recapitulate the tumor immune microenvironment of human BCa; the immunomodulatory role of the THAP7-AS1-IGF2BP3-CCN2 axis in the tumor microenvironment remains to be investigated. Finally, the clinical translatability of targeting THAP7-AS1 needs to be further evaluated in more clinically relevant models, such as patient-derived organoids and larger animal models. The findings of this study highlight several promising directions for future research. First, large-scale multi-center studies are warranted to validate the clinical utility of THAP7-AS1 as a diagnostic and prognostic biomarker for LN-metastatic BCa. Second, the full regulatory network of the THAP7-AS1-IGF2BP3 axis should be delineated via multi-omics approaches to identify additional downstream effectors involved in BCa progression. Third, the development of targeted therapeutic strategies against THAP7-AS1, such as antisense oligonucleotides (ASOs) or small interfering RNAs, should be explored in preclinical models to evaluate their efficacy against LN-metastatic BCa. Finally, the potential of the THAP7-AS1-IGF2BP3-CCN2 axis as a predictive biomarker for systemic therapy response in BCa patients warrants further investigation.

In summary, our study refines the conceptual framework by which lncRNAs and m^{6}A readers cooperate to shape metastatic competence and highlights the THAP7-AS1-IGF2BP3-CCN2 axis as a potential therapeutic vulnerability in LN-metastatic BCa.

Acknowledgements

This work was funded by the Fujian Provincial Clinical Key Specialty Construction Program (No. 0060112508), the Natural Science Foundation of Fujian Province, China (2021J01398), the National Science and Technology Major Project (matching grant from Fuzhou University Affiliated Provincial Hospital) and the Talent Introduction Startup Fund from Fuzhou University Affiliated Provincial Hospital (No. 00803216).

Disclosure of conflict of interest

None.

Address correspondence to: Liefu Ye, Shengli Clinical Medical College of Fujian Medical University, Fuzhou University Affiliated Provincial Hospital, No. 134, Dong street, Fuzhou 350001, Fujian, P. R. China. Tel: +86-13696885658; Fax: +86-0591-87532356; E-mail: yeliefu0122@163.com

References

[1] Witjes JA, Bruins HM, Cathomas R, Compérat EM, Cowan NC, Gakis G, Hernández V, Linares Espinós E, Lorch A, Neuzillet Y, Rouanne M, Thalmann GN, Veskimäe E, Ribal MJ and van der Heijden AG. European association of urology guidelines on muscle-invasive and metastatic bladder cancer: summary of the 2020 guidelines. Eur Urol 2021; 79: 82-104.

[2] Abufaraj M, Gust K, Moschini M, Foerster B, Soria F, Mathieu R and Shariat SF. Management of muscle invasive, locally advanced and metastatic urothelial carcinoma of the bladder: a literature review with emphasis on the role of surgery. Transl Androl Urol 2016; 5: 735-744.

[3] Lenis AT, Lec PM, Chamie K and Mshs M. Bladder cancer: a review. JAMA 2020; 324: 1980.

[4] Wang KC and Chang HY. Molecular mechanisms of long noncoding RNAs. Molecular Cell 2011; 43: 904-914.

[5] Mattick JS, Amaral PP, Carninci P, Carpenter S, Chang HY, Chen LL, Chen R, Dean C, Dinger ME, Fitzgerald KA, Gingeras TR, Guttman M, Hirose T, Huarte M, Johnson R, Kanduri C, Kapranov P, Lawrence JB, Lee JT, Mendell JT,

Mercer TR, Moore KJ, Nakagawa S, Rinn JL, Spector DL, Ulitsky I, Wan Y, Wilusz JE and Wu M. Long non-coding RNAs: definitions, functions, challenges and recommendations. Nat Rev Mol Cell Biol 2023; 24: 430-447.

[6] Shi M, Zhang R, Lyu H, Xiao S, Guo D, Zhang Q, Chen XZ, Tang J and Zhou C. Long non-coding RNAs: emerging regulators of invasion and metastasis in pancreatic cancer. J Adv Res 2025; 78: 285-306.

[7] Jiang X, Liu B, Nie Z, Duan L, Xiong Q, Jin Z, Yang C and Chen Y. The role of m6A modification in the biological functions and diseases. Sig Transduct Target Ther 2021; 6: 74.

[8] Wang X, Lu Z, Gomez A, Hon GC, Yue Y, Han D, Fu Y, Parisien M, Dai Q, Jia G, Ren B, Pan T and He C. N6-methyladenosine-dependent regulation of messenger RNA stability. Nature 2014; 505: 117-120.

[9] Huang H, Weng H, Sun W, Qin X, Shi H, Wu H, Zhao BS, Mesquita A, Liu C, Yuan CL, Hu YC, Hüttelmaier S, Skibbe JR, Su R, Deng X, Dong L, Sun M, Li C, Nachtergaele S, Wang Y, Hu C, Ferchen K, Greis KD, Jiang X, Wei M, Qu L, Guan JL, He C, Yang J and Chen J. Recognition of RNA N6-methyladenosine by IGF2BP proteins enhances mRNA stability and translation. Nat Cell Biol 2018; 20: 285-295.

[10] Zhou KI and Pan T. An additional class of m6A readers. Nat Cell Biol 2018; 20: 230-232.

[11] Lv L, Wei Q, Zhang J, Dong Y, Shan Z, Chang N, Zhao Y, Bian P and Yi Q. IGF2BP3 prevent HMGB1 mRNA decay in bladder cancer and development. Cell Mol Biol Lett 2024; 29: 39.

[12] Huang W, Zhu L, Huang H, Li Y, Wang G and Zhang C. IGF2BP3 overexpression predicts poor prognosis and correlates with immune infiltration in bladder cancer. BMC Cancer 2023; 23: 116.

[13] Kubota S and Takigawa M. Cellular and molecular actions of CCN2/CTGF and its role under physiological and pathological conditions. Clin Sci (Lond) 2015; 128: 181-196.

[14] Ramazani Y, Knops N, Elmonem MA, Nguyen TQ, Arcolino FO, van den Heuvel L, Levtchenko E, Kuypers D and Goldschmeding R. Connective tissue growth factor (CTGF) from basics to clinics. Matrix Biol 2018; 68-69: 44-66.

[15] Wang X, Xu T, Gao F, He H, Zhu Y and Shen Z. Targeting of CCN2 suppresses tumor progression and improves chemo-sensitivity in urothelial bladder cancer. Oncotarget 2017; 8: 66316-66327.

[16] Liu HT, Zou YX, Zhu WJ, Sen-Liu, Zhang GH, Ma RR, Guo XY and Gao P. lncRNA THAP7-AS1, transcriptionally activated by SP1 and post-transcriptionally stabilized by METTL3-mediated m6A modification, exerts oncogenic properties by improving CUL4B entry into the nucleus. Cell Death Differ 2022; 29: 627-641.

[17] Pei M, Yang Y, Su B, Li N, Zhao M, Zhao J, Yang T, Wang L, Quan S, Sun R and Yang X. LncTHAP7-AS1 suppresses the ovarian cancer progression by targeting miR-92b-5p/fatty acid 2-hydroxylase signal axis. Transl Oncol 2025; 61: 102514.

[18] Li P, Ma X and Gu X. The essential roles of lncRNAs/PI3K/AKT axis in gastrointestinal tumors. Front Cell Dev Biol 2024; 12: 1442193.

[19] Liu S, Chen X and Lin T. Lymphatic metastasis of bladder cancer: molecular mechanisms, diagnosis and targeted therapy. Cancer Letters 2021; 505: 13-23.

[20] Tian Z, Meng L, Wang X, Diao T, Hu M, Wang M, Zhang Y and Liu M. Predictive nomogram and risk factors for lymph node metastasis in bladder cancer. Front Oncol 2021; 11: 690324.

[21] Zhang C, Hu J, Li H, Ma H, Othmane B, Ren W, Yi Z, Qiu D, Ou Z, Chen J and Zu X. Emerging biomarkers for predicting bladder cancer lymph node metastasis. Front Oncol 2021; 11: 648968.

[22] Schmitt AM and Chang HY. Long noncoding RNAs in cancer pathways. Cancer Cell 2016; 29: 452-463.

[23] Fang Y and Fullwood MJ. Roles, functions, and mechanisms of long non-coding RNAs in cancer. Genomics Proteomics Bioinformatics 2016; 14: 42-54.

[24] Kopp F and Mendell JT. Functional classification and experimental dissection of long noncoding RNAs. Cell 2018; 172: 393-407.

[25] Mancarella C and Scotlandi K. IGF2BP3 from physiology to cancer: novel discoveries, unsolved issues, and future perspectives. Front Cell Dev Biol 2020; 7: 363.

[26] Liu X, Chen J, Chen W, Xu Y, Shen Y and Xu X. Targeting IGF2BP3 in cancer. Int J Mol Sci 2023; 24: 9423.

[27] Jiang CG, Lv L, Liu FR, Wang ZN, Liu FN, Li YS, Wang CY, Zhang HY, Sun Z and Xu HM. Downregulation of connective tissue growth factor inhibits the growth and invasion of gastric cancer cells and attenuates peritoneal dissemination. Mol Cancer 2011; 10: 122.

[28] Chien W, O'Kelly J, Lu D, Leiter A, Sohn J, Yin D, Karlan B, Vadgama J, Lyons KM and Koeffler HP. Expression of connective tissue growth factor (CTGF/CCN2) in breast cancer cells is associated with increased migration and angiogenesis. Int J Oncol 2011; 38: 1741-1747.

[29] Ubink I, Verhaar ER, Kranenburg O and Goldschmeding R. A potential role for CCN2/CTGF in aggressive colorectal cancer. J Cell Commun Signal 2016; 10: 223-227.

Supplementary Table 1. Correlation between *THAP7-AS1* expression and clinicopathologic characteristics of BCa patients (*n* = 200)

Characteristics	No. of cases	*THAP7-AS1* expression		
		Low	High	*P*-value[i]
Total cases	200	100	100	
Gender				0.136
Male	132	71	61	
Female	68	29	39	
Age				0.169
< 65	104	55	49	
≥ 65	96	60	36	
T grade				0.006**
Low	58	36	22	
High	142	58	84	
Lymphatic metastasis				
Negative	144	91	53	0.001**
Positive	56	9	47	

Abbreviations: No. of cases = number of cases; T grade = tumor grade. [i]Chi-square test, ***P* <0.01.

Supplementary Table 2. Univariate and multivariate analysis of Overall Survival for *THAP7-AS1* expression in patients with BCa (*n* = 200)

Variables	Univariate analysis			Multivariate analysis		
	HR	95% CI	*P*-value[i]	HR	95% CI	*P*-value[i]
Age (<65 vs. ≥65)	1.18	0.84-1.66	0.34			
Gender (Male vs. Female)	1.10	0.78-1.56	0.59			
T grade (High vs. Low)	1.26	0.87-1.83	0.22			
Lymphatic metastasis (Positive vs. Negative)	2.32	1.62-3.33	0.001**	1.98	1.34-2.93	0.001**
THAP7-AS1 expression (High vs. Low)	2.05	1.45-2.90	0.001**	1.76	1.23-2.51	0.002**

Abbreviations: HR = hazard ratio; 95% CI = 95% confidence interval; T grade = tumor grade. [i]Cox regression analysis, ***P* <0.01.

Supplementary Table 3. Univariate and multivariate analysis of Disease-Free Survival for *THAP7-AS1* expression in patients with BCa (*n* = 200)

Variables	Univariate analysis			Multivariate analysis		
	HR	95% CI	*P*-value[i]	HR	95% CI	*P*-value[i]
Age (<65 vs. ≥65)	1.21	0.87-1.68	0.26			
Gender (Male vs. Female)	1.08	0.77-1.51	0.65			
T grade (High vs. Low)	1.29	0.91-1.84	0.15			
Lymphatic metastasis (Positive vs. Negative)	2.45	1.74-3.46	0.001**	2.10	1.47-3.01	0.001**
THAP7-AS1 expression (High vs. Low)	2.18	1.57-3.03	0.001**	1.84	1.30-2.61	0.001**

Abbreviations: HR = hazard ratio; 95% CI = 95% confidence interval; T grade = tumor grade. [i]Cox regression analysis, ***P* <0.01.

Supplementary Table 4. Primers and probes used in the experiments

Gene	Sequence (5'-3')	Application
THAP7-AS1	F: TGGGACGCTTGCACGAAAGA R: GCGATACTGTCTTTCTCCTG	qRT-PCR
GAPDH	F: CACATCGCTCAGACACCATG R: TGACGGTGCCATGGAATTTG	qRT-PCR
U1	F: GGAGATACCATGATCACGAAGG R: CATCCGGAGTGCAATGGATAAG	qRT-PCR
CCN2	F: GCGTGTGCACCGCCAAAGAT R: CAGGGCTGGGCAGACGAACG	qRT-PCR
TGFB3	F: ATGCCAAAGAAATCCATAAATTC R: GAAGCGGAAAACCTTGGAGGTA	qRT-PCR
IGF2BP3	F: AGCGTGGAGAAAGGACGAGA R: GGCCATCTTGGTGTCACTGA	qRT-PCR
si-IGF2BP3#1	sense: GGAUCUUACUGGACAGAAAGA antisense: UCUUUCUGUCCAGUAAGAUCC	si-RNA
si-IGF2BP3#2	sense: GCUACAGUUGGAGAUUGAAGA antisense: UCUUCAAUCUCCAACUGUAGC	si-RNA
si-THAP7-AS1#1	sense: GGAAGUACCUUGAGAAUCUCA antisense: UGAGAUUCUCAAGGUACUUCC	si-RNA
si-THAP7-AS1#2	sense: GCUUGAGAAAGACCUUGAUAA antisense: UUAUCAAGGUCUUUCUCAAGC	si-RNA
si-METTL3#1	sense: GCAAGUAUGUUCACUAUGATT antisense: UCAUAGUGAACAUACUUGCAG	si-RNA
si-METTL3#2	sense: GGAAGACAUUGAUGAGAAUCA antisense: UGAUUCUCAUCAAUGUCUUCC	si-RNA
THAP7-AS1	TCCAAACCAACTTGGTGCCATACC 5'-Cy3 labeled and 3'-Cy3 labeled	FISH

Supplementary Table 5. Antibodies used in the experiments

Product	Source	No. of Catalogue
Western blot		
anti-IGF2BP3	Abcam	ab177477
anti-GAPDH	Beijing Ray Antibody Biotech	RM2002
anti-CCN2	Abcam	ab6992
IF		
anti-LYVE-1	Abcam	ab218535
anti-IGF2BP3	Abcam	ab177477
anti-CCN2	Abcam	ab6992
anti-PanCK	Abcam	ab7753
IP		
anti-IGF2BP3	Abcam	ab177477
anti-IgG	Thermo Fisher Scientific	MA1-81209
anti-m6A	Proteintech	68055-1
Secondary antibody		
Western blot		
anti-rabbit IgG-HRP	Cell Signaling Technology	7074
anti-mouse IgG-HRP	Cell Signaling Technology	7076

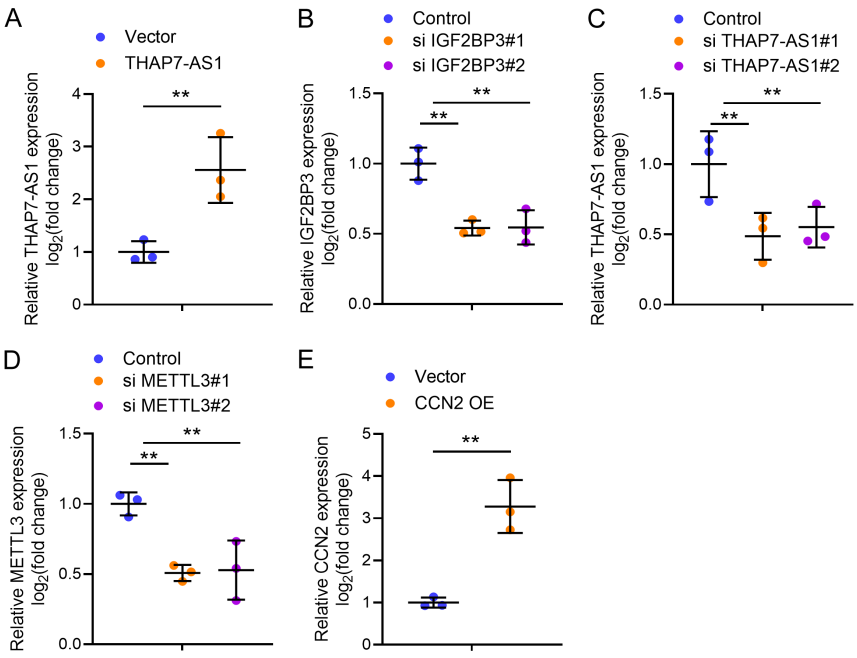

Supplementary Figure 1. Efficient modulation of THAP7-AS1, IGF2BP3, METTL3 and CCN2 expression in BCa cells. A. qRT-PCR analysis of THAP7-AS1 expression in BCa cells after THAP7-AS1 overexpression. Error bars show the mean ± SD, **P < 0.01 by nonparametric Mann-Whitney *U* test. B. qRT-PCR analysis of IGF2BP3 expression in BCa cells after IGF2BP3 knockdown. Error bars show the mean ± SD, **P < 0.01 by one-way ANOVA followed by Dunnett's tests. C. qRT-PCR analysis of THAP7-AS1 expression in BCa cells after THAP7-AS1 knockdown. Error bars show the mean ± SD, **P < 0.01 by one-way ANOVA followed by Dunnett's tests. D. qRT-PCR analysis of METTL3 expression in BCa cells after METTL3 knockdown. Error bars show the mean ± SD, **P < 0.01 by one-way ANOVA followed by Dunnett's tests. E. qRT-PCR analysis of CCN2 expression in BCa cells after CCN2 overexpression. Error bars show the mean ± SD, **P < 0.01 by nonparametric Mann-Whitney *U* test.